Genesis of Bimetallic Pt−Cu Clusters in Reverse Micelles Investigated by in Situ X-ray Absorption Spectroscopy

Bing-Joe Hwang,*,† Yin-Wen Tsai,† Loka Subramanyam Sarma,† Yu-Li Tseng,† Din-Goa Liu,‡ and Jyh-Fu Lee‡

Nanoelectrochemistry Laboratory, Department of Chemical Engineering, National Taiwan University of Science and Technology, Taipei 106, Taiwan, Republic of China

Received: September 16, 2004

The formation mechanism of platinum−copper (Pt−Cu) bimetallic clusters at the early stage within the water-in-oil microemulsion system of water/sodium bis(2-ethyl hexyl)sulfosuccinate/*n*-heptane is explored by in situ X-ray absorption spectroscopy. The reduction of platinum and copper ions and the formation of corresponding clusters are monitored as a function of the dosage of reducing agent, hydrazine (N_2H_4). Upon successive addition of the reducing agent, hydrazine (N_2H_4), five distinguishable steps are observed in the formation process of Pt−Cu clusters at the early stage. Both in situ X-ray absorption near-edge structure and extended X-ray absorption fine structure at the Pt L_{III}-edge suggest the $Pt^{4+} \rightarrow Pt^{2+} \rightarrow Pt^0$ reduction sequence, and analysis of the spectra recorded at the Cu K-edge confirms the $Cu^{2+} \rightarrow Cu^0$ reduction sequence. A corresponding structural model is proposed for each step to provide detailed insight into the mechanism of nucleation and growth of Pt−Cu bimetallic clusters.

Introduction

Bimetallic clusters are of great interest from both a scientific and a technological perspective for the modification of physical and chemical properties of metal particles.[1−4] Bimetallic catalysts usually exhibit unique catalytic performances such as enhanced activity, selectivity, and stability as compared to the separate components.[1] The activity and selectivity of the metal catalysts can be drastically affected by the presence of a second metal component.[5,6] The presence of a second metal causes morphological variations, changes in physical and chemical interactions among different atoms, and can provide new properties to the bi- or multimetallic nanoparticles. Controlling the size and morphology of a metal nanoparticle is an extremely important aspect of nanoparticle research as it has a strong influence on optical, magnetic, electronic, and catalytic properties of the nanoparticles. The materials synthesized from micellar solutions of surfactants, which combine the advantages of high specific surface area and uniform particle size distribution, are of paramount interest for applications in catalysis and fuel cells. Because nanotechnology is regarded as a major future technology, methods of scaling-up nanoparticle synthesis become highly desired. Thorough understanding of the formation mechanism is necessary to control the size, shape, and surface morphology of the nanoparticles (factors which govern the catalytic activity of the nanoparticles). Success in either particle design or scaling-up also requires a detailed knowledge of the particle formation mechanism. Although a large number of studies were focused on the synthesis and characterization of bimetallic clusters, e.g., Ag−Cu and Au−Cu,[7] Pd−Pt,[8] Au−Pd,[9] Pd−Au,[10] Pt−Ru,[11,12] Rh−Pt,[13] and Pd−Au,[14] we know of no reports focusing on the formation mechanism of bimetallic clusters at early stages. One of the methods suitable to study the structure of metal clusters is the in situ XAS (X-ray absorption spectroscopy) comprising both near-edge (XANES) and extended absorption fine structure (EXAFS) regions. This technique is specific to the study on colloidal dispersions of metallic clusters, since it is difficult to obtain structural information on such systems by means of a conventional diffraction method at the early stages. Moreover, because of the change in cluster structure during the course of formation, ex situ techniques such as transmission electron microscopy and X-ray diffraction are difficult to give the real-time structural information. Recently, we have successfully evaluated the formation mechanism of Pt clusters in sodium bis(2-ethyl hexyl)sulfosuccinate (AOT) reverse microemulsions by in situ XAS.[15] From an analysis of the EXAFS data, one can determine the local structure around a specific type of atom. In line with our ongoing effort for the evaluation of a formation mechanism of metal nanoparticles, we have aimed here to investigate the formation mechanism of Pt−Cu bimetallic clusters by in situ XAS at the early stages. By analyzing the EXAFS spectra of Pt−Cu bimetallic clusters at the Pt L_{III}-edge and Cu K-edge, we are able to propose a formation mechanism by determining the parameters such as coordination number (N), bond distance (R), and static and dynamic disorder (σ_j^2) during the course of the formation of Pt−Cu clusters.

Experimental Section

Preparation of Pt−Cu Clusters in AOT Reverse Micelles. The bimetallic Pt−Cu clusters were prepared in microemulsions containing *n*-heptane as the continuous oil phase, AOT (99%) as a surfactant, and either Pt or Cu precursor solutions or hydrazine solution as the dispersed aqueous phase. The Pt precursor, $H_2PtCl_6 \cdot 6H_2O$ (0.1571 g), was dissolved in 0.42 mL of water, which gives a Pt^{4+} concentration of 0.72 M, and to this 5 mL of 1 M AOT in *n*-heptane was added to form a microemulsion with the Pt complex in the water pool. Similarly,

* To whom correspondence should be addressed. Fax: +886-2-27376644. E-mail: bjh@ch.ntust.edu.tw.
† National Taiwan University of Science & Technology.
‡ National Synchrotron Radiation Research Center, Hsinchu 300, Taiwan.

10.1021/jp045802l CCC: $27.50
Published on Web 11/26/2004

the Cu precursor $Cu(NO_3)_2 \cdot 2H_2O$ (0.0569 g) was dissolved in 0.42 mL of water, which gives a Cu^{2+} concentration of 0.72 M, and to this 5 mL of 1 M AOT in *n*-heptane was added to form a microemulsion with the Cu complex in the water pool. The Pt and Cu complex microemulsions were then mixed together to form a Pt−Cu complex microemulsion. The molar ratio of water to surfactant was equal to 4.55, the aqueous phase contained 0.36 M Pt^{4+} as well as Cu^{2+} ions, and the amount of both of the ions was equal to 2.952×10^{-4} mol. A microemulsion of the same composition of oil, water, and the surfactant that contained the reducing agent, hydrazine (N_2H_4), was also prepared. This microemulsion was then added to the other microemulsion containing the Pt−Cu complex, whereby the Pt−Cu complex was reduced. All reactions were carried out at 298 K unless otherwise specified.

In Situ XAS Measurements. The X-ray absorption spectra were recorded at the Beam Line 17C at the National Synchrotron Radiation Research Center (NSRRC), Hsinchu, Taiwan. The electron storage ring was operated at 1.5 GeV with a beam current of 100−200 mA. A double Si(111) crystal monochromator was employed for energy selection. One collimating mirror and one refocusing mirror, both coated with Rh, were respectively located upstream and downstream of the monochromator. These two mirrors also served to reject high harmonics. The focused beam size at the sample position was 4×2 mm^2. Formation of Pt−Cu clusters in reverse micelles proceeded in a homemade liquid cell for in situ XAS study. This in situ cell was carefully designed to avoid excessive attenuation of the X-ray beam. A hollow Teflon rod with Kapton film capped at one end was inserted into the in situ XAS cell to adjust the thickness of the liquid layer so that the proper edge jump step could be achieved during the measurements. All of the spectra were collected in the transmission mode with three gas-filled ionization chambers. The third ion chamber was used in conjunction with the reference sample, which was a Pt foil for Pt L_{III}-edge measurements and a Cu foil for Cu K-edge measurements.

XAS Data Analysis. Standard procedures were followed to analyze the EXAFS data. First, the raw absorption spectrum in the preedge region was fit to a straight line and the background above the edge was fit with a cubic spline. The EXAFS function, χ, was obtained by subtracting the postedge background from the overall absorption and then normalizing with respect to the edge jump step. The normalized $\chi(E)$ was transformed from energy space to *k*-space, where "*k*" is the photoelectron wave vector. The $\chi(k)$ data were multiplied by k^3 to compensate for the damping of EXAFS oscillations in the high-*k* region. Subsequently, k^3-weighted $\chi(k)$ data in the *k*-space ranging from 3.00 to 14.00 Å^{-1} for the Pt L_{III}-edge and from 3.45 to 11.55 Å^{-1} for the Cu K-edge were Fourier-transformed (FT) to *r* space to separate the EXAFS contributions from different coordination shells. A nonlinear least-squares algorithm was applied to curve fitting of EXAFS in *R* space between 1.25 and 2.39 Å (without phase correction) for the Pt L_{III}-edge and between 0.75 and 2.0 Å for the Cu K-edge. All of the computer programs were implemented in the UWXAFS 3.0 package[16] with the backscattering amplitude and the phase shift for the specific atom pairs being theoretically calculated by using FEFF7 code.[17]

Results and Discussion

In Situ XANES at the Pt L_{III}-Edge of Pt−Cu Bimetallic Clusters. In XAS, the energy region in the vicinity of the absorption edge (0−50 eV) is referred to as XANES and it is to a large extent a fingerprint for the oxidation state and site

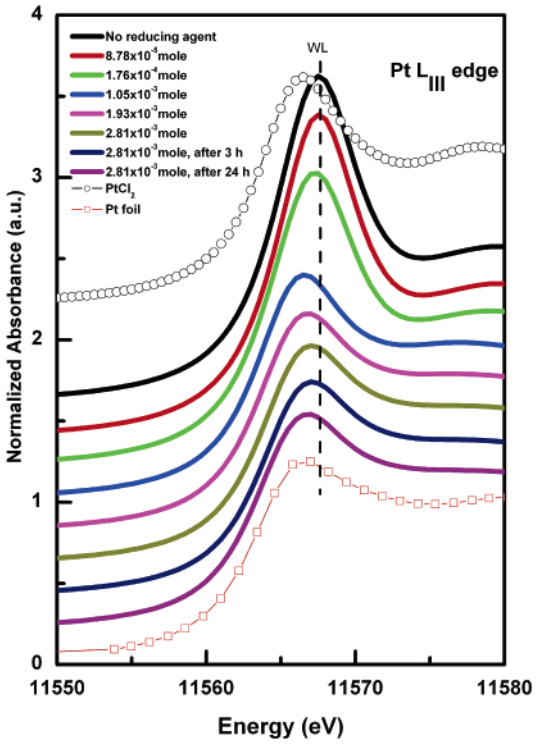

Figure 1. Normalized absorption spectra near the Pt L_{III}-edge of the Pt−Cu bimetallic microemulsion system.

TABLE 1: Edge Energies and White Line Areas of the Pt−Cu Microemulsion System at the Pt L_{III}-Edge as a Function of N_2H_4 Dosage

	Pt L_{III}-edge		
amount of N_2H_4 (mol)	energy of absorption edge (eV)	energy of main peak (eV)	area of the white line
0	11565.5	11567.5	5.673
8.78×10^{-5}	11565.5	11567.5	5.627
1.76×10^{-4}	11565	11567.5	4.497
1.05×10^{-3}	11564.5	11567.5	2.239
1.93×10^{-3}	11564.5	11567	1.814
2.81×10^{-3}	11564.5	11567	1.624
2.81×10^{-3}, 3 h	11564.5	11567	1.488
2.81×10^{-3}, 24 h	11564	11567	1.177
$PtCl_2$ reference	11564	11566.5	2.716
Pt foil	11564	11566	1.179

symmetry of the element from which the absorption spectrum was measured. In Pt XANES, the sharp peak (the so-called white line) at the Pt L_{III}-edge is an absorption threshold resonance, which is attributed to the electronic transitions that arise when an incident electron excites a $2p_{3/2}$ (L_{III}-edge) core electron to the unoccupied "d" states near or above the Fermi level and is sensitive to the degree of electron occupancy in the valence orbits of the absorber.[18] Generally speaking, the lower the white line intensity, the higher the electron density and the lower the oxidation state of the Pt. Hence, changes in the white line intensity may be regarded as an indication of the change in the oxidation state of the Pt atom. This point is clearly demonstrated by the white line intensity difference between the H_2PtCl_6 solution in the microemulsion and during the progressive addition of N_2H_4 as shown in the Figure 1. The white line intensity at all of the conditions studied, reference $PtCl_2$, and the Pt foil along with the edge energies are shown in Table 1.

The intensity of the white line peak (represented as WL) was found to be 5.674 in the absence of the reducing agent and shows little change (5.627) when 8.78×10^{-5} mol of reducing

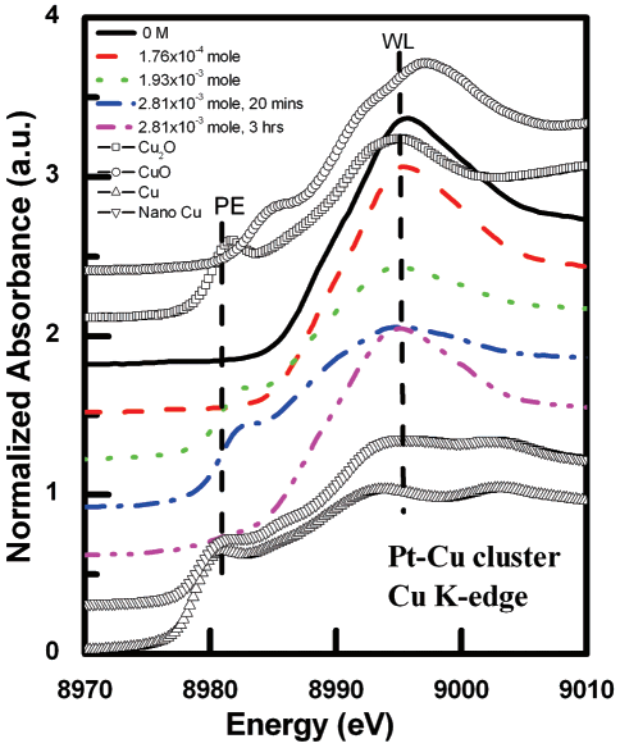

Figure 2. XANES spectra at the Cu K-edge of the Pt−Cu microemulsion system as a function of hydrazine dosage.

TABLE 2: Edge Energies and White Line Areas of the Pt−Cu Microemulsion System at the Cu K-Edge as a Function of N_2H_4 Dosage

	Cu K-edge		
amount of N_2H_4 (mol)	energy of absorption edge (eV)	energy of main peak (eV)	area of the white line
0	8988.2	8995.2	7.169
1.76×10^{-4}	8988.2	8995.5	6.751
1.93×10^{-3}	8987.8	8995.1	2.817
2.81×10^{-3}, 20 min	8980.8	8994.7	2.520
2.81×10^{-3}, 3 h	8980.8	8994.7	5.154
CuO reference	8983.7	8997.2	3.536
Cu foil	8979	8994.2	0.853

agent is added. The area of the white line decreases drastically to 2.239 as the reducing agent dosage increases from 8.78×10^{-5} to 1.05×10^{-3} mol due to the decrease in the density of unoccupied d states. At this stage, the XANES pattern is similar to that of the $PtCl_2$ reference. This indicates the gradual change in the Pt oxidation state from +4 to +2. A further increase in the dosage of the reducing agent decreases the white line intensity. At 2.81×10^{-3} mol of N_2H_4 and after having been kept for 24 h, the white line intensity (1.177) is almost similar to the white line intensity of the Pt foil (1.179), which indicated further reduction of the Pt ions from Pt^{2+} to Pt^0 and formation of Pt clusters in the microemulsion system, and these results are consistent with our previous report,[15] in which we have demonstrated the stepwise reduction sequence of $Pt^{4+} \rightarrow Pt^{2+} \rightarrow Pt^0$ during Pt clusters formation in AOT reverse micelles.

In Situ XANES at the Cu K-Edge of Pt−Cu Bimetallic Clusters. Figure 2 displays the spectra near the Cu K-edge of the microemulsion system as a function of the dosage of reducing agent, N_2H_4, and Table 2 lists the white line areas at all of the conditions studied along with the edge energies. The dominant XANES peak (white line, represented as WL) at the Cu K-edge is an absorption threshold resonance, which is assigned to the allowed 1s → 4p transition[19] and is an immediate indication of the oxidation state of Cu. Hence, changes in the white line intensity indicate the changes in the oxidation state of Cu atom. The preedge peak (represented as PE) that appeared below the WL from 8975 to 8982 is attributed to the 1s → 3d transition.[20] As can be seen in this figure, the intensity of the white line decreases gradually as the dosage of the reducing agent increases from 1.76×10^{-4} to 2.81×10^{-3} mol and after having been kept for 20 min.

In the absence of N_2H_4, the white line area is found to be 7.169 and decreased sharply to 2.520 upon addition of 2.81×10^{-3} mol of N_2H_4 and after having been kept for 20 min. The edge energy of the Pt−Cu microemulsion system after having been kept for 20 min in the presence of hydrazine of 2.81×10^{-3} mol is found to be similar to that of nano Cu. This evidence indicated that copper ions are reduced from Cu^{2+} to Cu^0. For the purpose of comparison, Cu K-edge spectra of some reference materials such as Cu_2O, CuO, bulk Cu, and nano Cu are also shown in Figure 2. From the EXAFS data analysis (see below), a lower Cu−Pt coordination envisages that the Cu^0 species are speculated to be adsorbed on the surface of Pt clusters. Another reason is that the equilibrium potentials (E_0) of the electrochemical reactions $[PtCl_6]^{2-} + 2\ e^- \rightarrow [PtCl_4]^{2-} + 2\ Cl^-$, 0.68 V, and $[PtCl_4]^{2-} + 2\ e^- \rightarrow Pt + 4\ Cl^-$, 0.755 V, are substantially higher than that of the equilibrium potential of the electrochemical reaction $Cu^{2+} + 2\ e^- \rightarrow Cu$, 0.34 V.[21]

The higher equilibrium potential for platinum indicates that platinum ions would be preferentially reduced when a reducing agent is added to an aqueous solution containing a mixture of platinum and copper ions. Hence, the formation of bulk Pt−Cu nanoparticles can be least favorable in our present investigation. It is noteworthy that some spectral features of nano Cu are different from those of bulk Cu foil. This may be due to the availability of a higher percentage of Cu atoms on the surface.[22] If the Pt−Cu microemulsion system is allowed to stand for 3 h in the presence of 2.81×10^{-3} mol of hydrazine, the XANES features reveal the reoxidation of copper. An intense band at 8995−9000 eV that appeared in the XANES spectra can be attributed to the 1s → 4p transition that indicates the existence of Cu(II), suggesting that Cu is dissolved from the Pt surface to form oxidized species. This situation will be discussed later.

In Situ EXAFS at the Pt L_{III}-Edge of Pt−Cu Clusters. Figure 3 shows the k^3-weighted EXAFS spectra at the Pt L_{III}-edge of the Pt−Cu microemulsion system. A high signal-to-noise ratio of the data allows EXAFS oscillations to be clearly observed up to 15 $Å^{-1}$. It is found that the magnitude of oscillations decreased with the increasing dosage of reducing agent. Figure 4 shows the radial distribution function around the Pt atom obtained by taking FTs of the EXAFS data.

The main peak in Figure 4 can be assigned to the Pt−Cl bond with an interatomic distance of approximately 2.32 Å. Another peak observed around 2.5 Å is attributed to the Pt−Pt bond. The contribution of the Pt−Cl bond decreases gradually with an increasing dosage of reducing agent while the magnitude of the Pt−Pt peak increases gradually. These observations indicate the reduction of Pt ions and the formation of Pt clusters by the addition of reducing agent. The structural parameters including the coordination number (N), bond distance (R), Debye−Waller factor (σ^2), and inner potential shift (ΔE_0) derived from the Pt L_{III}-edge EXAFS data analysis are listed in Table 3.

The coordination number of Cl around Pt is found to be 6 in the absence of reducing agent. This value is subjected to negligible change even after the addition of reducing agent of 8.78×10^{-5} mol. However, the Pt−Cl coordination number is

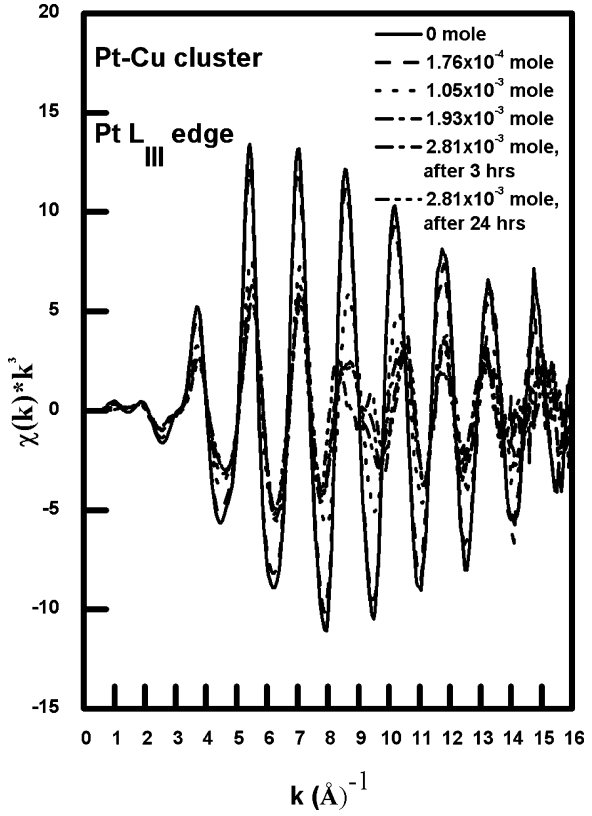

Figure 3. k^3-weighted EXAFS data at the Pt L_{III}-edge of the Pt−Cu bimetallic microemulsion system as a function of N_2H_4 dosage.

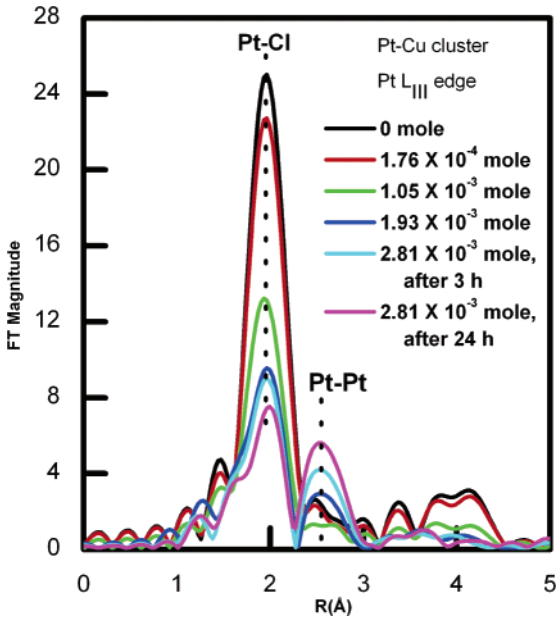

Figure 4. FT of EXAFS data in Figure 3, uncorrected for phase shift.

reduced to 3.5 when the dosage of N_2H_4 increased to 1.05×10^{-3} mol. Thereafter, the N_{Pt-Cl} value does not change further until the dosage of N_2H_4 exceeds 2.81×10^{-3} mol. In this stage, EXAFS results imply the reduction of Pt^{4+} to Pt^{2+} species as indicated by the following reactions:

$$0.5N_2H_4 \rightarrow 0.5N_2 + 2H^+ + 2e \quad (1)$$

$$2PtCl_6^{2-} + 2e \rightarrow 2PtCl_4^{2-} + 2Cl^- \quad (2)$$

The Pt−Pt bonds could be observed only after adding the reducing agent of more than 1.93×10^{-3} mol. The Pt−Pt coordination numbers are found to be 1.2, 2.4, and 3.5, respectively, with the reducing agent contents of 1.93×10^{-3}, 2.81×10^{-3} (3 h), and 2.81×10^{-3} (24 h) mol. This evidence indicates the formation of Pt clusters via further reduction of $PtCl_4^{2-}$ (Pt^{2+}) to Pt^0. The corresponding chemical reaction can be written as follows:

$$N_2H_4 + 2PtCl_4^{2-} \rightarrow N_2 + 2Pt^0 + 8Cl^- + 4H^+ \quad (3)$$

TABLE 3: Structural Parameters Derived from the Pt L_{III}-Edge EXAFS Data Analysis of the Pt−Cu Bimetallic Microemulsion System with Various Contents of Reducing Agent[a]

amount of N_2H_4 (mol)	shells	N	R_j (Å)	σ_j (Å^2) $\times 10^{-3}$	ΔE_0 (eV)	R factor
0	Pt−Cl	6 (0.4)	2.33	2.6 (0.4)	12.9 (0.8)	0.002
	Pt−Pt					
8.78×10^{-5}	Pt−Cl	5.7 (0.4)	2.33	2.6 (0.4)	12.9 (0.8)	0.002
	Pt−Pt					
1.76×10^{-4}	Pt−Cl	5.3 (0.4)	2.33	2.7 (0.4)	12.7 (0.9)	0.002
	Pt−Pt					
1.05×10^{-3}	Pt−Cl	3.5 (0.4)	2.31	3.7 (0.8)	12.9 (1.5)	0.006
	Pt−Pt					
1.93×10^{-3}	Pt−Cl	3.8 (0.5)	2.31	6.9 (0.5)	14.3 (0.9)	0.023
	Pt−Pt	1.2 (0.9)	2.69	5.1 (2.9)	−4.2 (9.2)	0.023
2.81×10^{-3}, 3 h	Pt−Cl	3.3 (0.7)	2.31	6.8 (0.7)	13.7 (1.2)	0.03
	Pt−Pt	2.4 (1.3)	2.69	6.1 (2.1)	−4.0 (6.4)	0.03
2.81×10^{-3}, 24 h	Pt−Cl	3.6 (1.0)	2.33	9.9 (1.1)	16.8 (1.5)	0.034
	Pt−Pt	3.5 (1.4)	2.69	6.4 (1.6)	6.4 (1.6)	0.034

[a] $k = 3-14$ Å^{-1}, $R = 1.25-2.39$ Å.

At this stage, we have expected the formation of bimetallic nanoparticles of a Pt-rich core and a Cu-rich shell type. Interestingly, we have observed the Pt−Cl coordination even after the formation of Pt clusters. This is probably due to the adsorption of Cl^- ions on the Pt clusters. On the other hand, no Cu coordination around Pt could be observed in the Pt−Cu microemulsion system with 2.81×10^{-3} mol of reducing agent. On the basis of our understanding of the state of Cu adsorbed on Pt clusters,[23] it is speculated that the Cu atoms were oxidized and dissolved from the surface of Pt clusters. This might be the reason that we always failed to observe the Cu coordination here. The detailed mechanism of this phenomenon will be discussed later.

In Situ EXAFS at the Cu K-Edge of Pt−Cu Clusters. Figure 5 shows the k^3-weighted EXAFS spectra at the Cu K-edge of the Pt−Cu microemulsion system. FTs of the k^3-weighted EXAFS spectra are shown in Figure 6. The main peak observed in this figure can be assigned to the contribution of the Cu−O bonds. It is worth noting that the Cu−Pt bond could not be identified even after the addition of reducing agent up to 2.81×10^{-3} mol (same observation from EXAFS at the Pt L_{III}-edge). More specifically, the contribution from the Cu−Pt bonds was found around 2.3 Å (without phase correction) only after having kept this microemulsion system for 20 min.

Interestingly, the contribution from the Cu−Pt bonds disappeared if the system is allowed to stand for 3 h, probably due to the dissolution of copper from the Pt surface. We checked the reliability of the Cu−Pt bond that arises when the microemulsion system with 2.81×10^{-3} mol of reducing agent after having been kept for 20 min is fit to the FEFF theory to the back-transformed experimental EXAFS data, and this is shown in Figure 7; good fit quality indicates that the Cu−Pt bond is reliable.

Table 4 lists the structural parameters derived from the Cu K-edge EXAFS data analysis of the Pt−Cu microemulsion system. The coordination number of O around Cu is found to

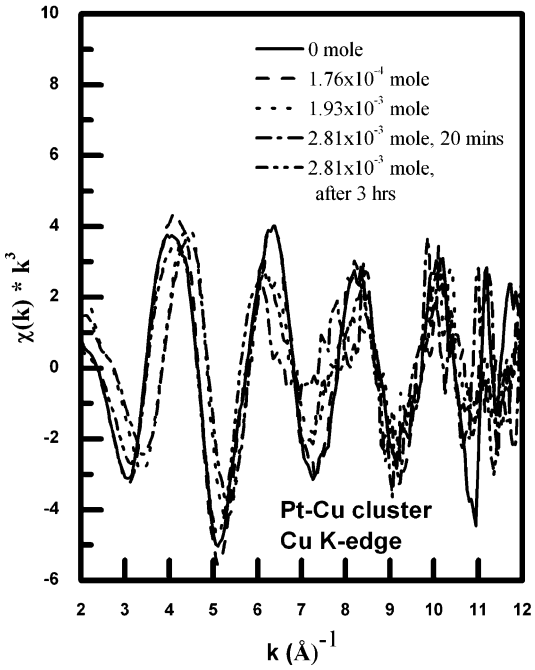

Figure 5. k^3-weighted EXAFS data at the Cu K-edge of the Pt−Cu bimetallic microemulsion system as a function of N_2H_4 dosage.

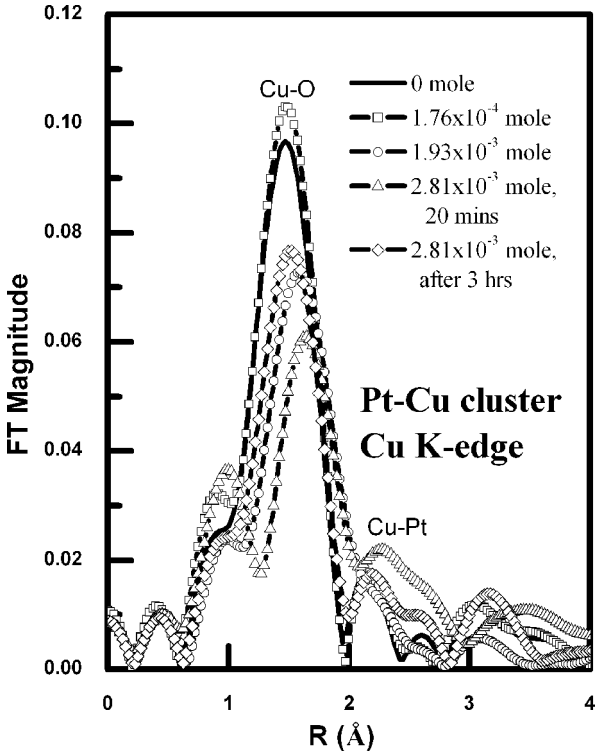

Figure 6. FT EXAFS spectra at the Cu K-edge of the Pt−Cu microemulsion system as a function of N_2H_4 dosage.

be 3.7 in the absence of reducing agent. The value of N_{Cu-O} does not change significantly even after the addition of 2.81×10^{-3} mol of reducing agent. For example, this value is slightly reduced to 3.3 after the Pt−Cu microemulsion system with 2.81×10^{-3} mol of reducing agent kept for 3 h. The coordination of Pt around Cu could be observed only for the Pt−Cu microemulsion system containing 2.81×10^{-3} mol of reducing agent and after being kept for 20 min. All of the observations indicated the adsorption of Cu on the Pt surface and the formation of Pt−Cu clusters via the reduction of Cu^{2+} to Cu^0.

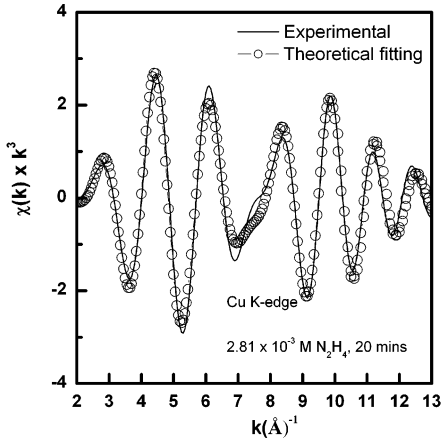

Figure 7. Two-shell fits (circle line) with the backtransformed experimental data (solid line) of Figure 6 at the Cu K-edge of the Pt−Cu microemulsion system with 2.81×10^{-3} mol of reducing agent after 20 min.

TABLE 4: Structural Parameters Derived from the Cu K-Edge EXAFS Data Analysis of the Pt−Cu Bimetallic Microemulsion System with Various Contents of Reducing Agent[a]

amount of N_2H_4 (mol)	shells	N	R_j (Å)	σ_j (Å^2) $\times 10^{-3}$	ΔE_0 (eV)	R factor
0	Cu−O	3.7 (1.1)	1.98	4.9 (2.6)	0.6 (4.1)	0.035
	Cu−Pt					
1.76×10^{-4}	Cu−O	4.5 (0.4)	1.96	6.3 (0.8)	−1.6 (1.2)	0.028
	Cu−Pt					
1.93×10^{-3}	Cu−O	3.1 (0.7)	2.00	6.9 (2.5)	9.8 (2.8)	0.022
	Cu−Pt					
2.81×10^{-3},	Cu−O	2.5 (1.5)	2.06	6.8 (1.1)	16.2 (1.1)	0.033
20 min	Cu−Pt	1.3 (0.7)	2.60	4.9 (2.6)	−28.3 (6.5)	0.033
2.81×10^{-3}, 3 h	Cu−O	3.3 (0.9)	1.99	5.5 (2.7)	−4.3 (4.5)	0.034
	Cu−Pt					

[a] $k = 3.45-11.55$ Å^{-1}, $R = 0.75-2.0$ Å.

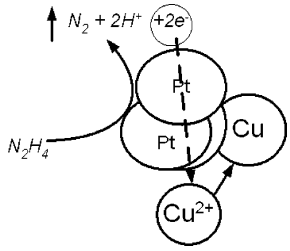

Figure 8. Formation mechanism of the Pt−Cu cluster.

Electrons required for this reduction come from the oxidation of the reducing agent as depicted in eq 1. The chemical reaction can be written as below:

$$Cu^{2+} + 2e^- \xrightarrow{\text{Pt Clusters}} Cu \qquad (4)$$

The process of formation of Cu on the Pt surface appeared as an electrochemical reaction. Hwang and Lin have already proposed this type of electrochemical mechanism for electroless deposition of cobalt on activated highly oriented pyrolytic graphite.[24] The Pt−Cu bimetallic cluster formation is schematically represented in Figure 8.

However, it is important to note that no coordination of Pt around Cu could be observed in the same solution after having been kept for 3 h. Dissolution of Cu can be explained as follows. When the Pt−Cu microemulsion system with reducing agent was kept for 3 h, all of the reducing agents would decompose to N_2, and then, the dissolved oxygen would be reduced on the

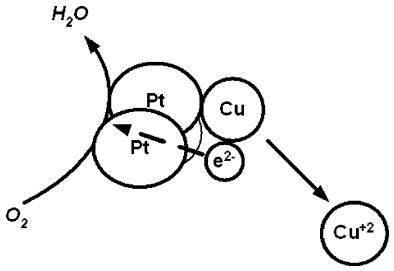

Figure 9. Dissolution of Cu from the Pt−Cu cluster and oxygen reduction on Pt.

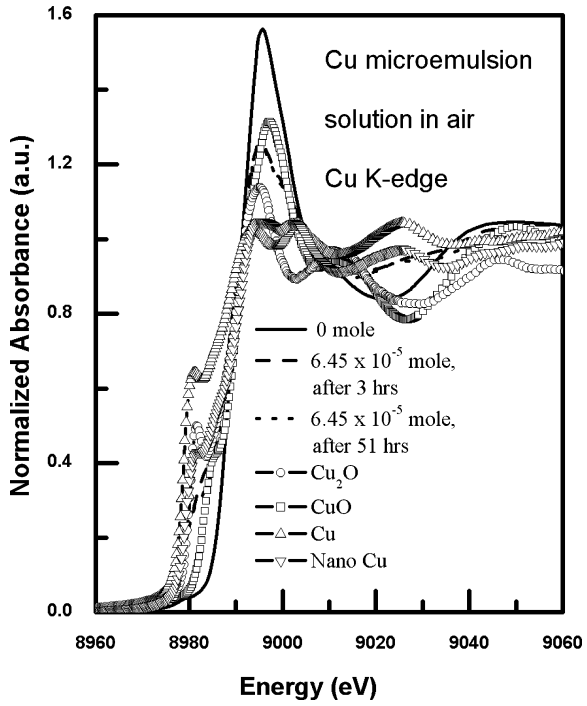

Figure 10. Normalized absorption spectra at the Cu K-edge of the Cu monometallic microemulsion system in air.

Pt surface since Pt is an effective catalyst for oxygen reduction.[25,26] The electrons required for this reduction would come from the dissolution of Cu. The dissolution process and the oxygen reduction occur as shown in the following equations (5 and 6), respectively:

$$Cu \rightarrow Cu^{2+} + 2e^- \quad (5)$$

$$O_2 + 4H^+ + 4e^- \rightarrow 2H_2O \quad (6)$$

A schematic representation of these reactions is shown in Figure 9. This is the reason that the coordination of Pt around Cu could not be observed for the Pt−Cu microemulsion system with a reducing agent after standing for 3 h.

From the above inference, Cu should not be dissolved in the absence of Pt clusters even with oxygen in the Pt−Cu microemulsion system. To clarify this inference, we have performed the XANES analysis for the Cu monometallic microemulsion system in the presence of air for a prolonged period and the results are shown in Figures 10 and 11. As can be seen from Figure 10 in the absence of reducing agent, the white line appeared at ∼8995 eV and the intensity decreased after 6.45×10^{-5} mol of N_2H_4 was added and kept for 3 h. However, the white line intensity did not further change even after the microemulsion system with 6.45×10^{-5} mol of N_2H_4

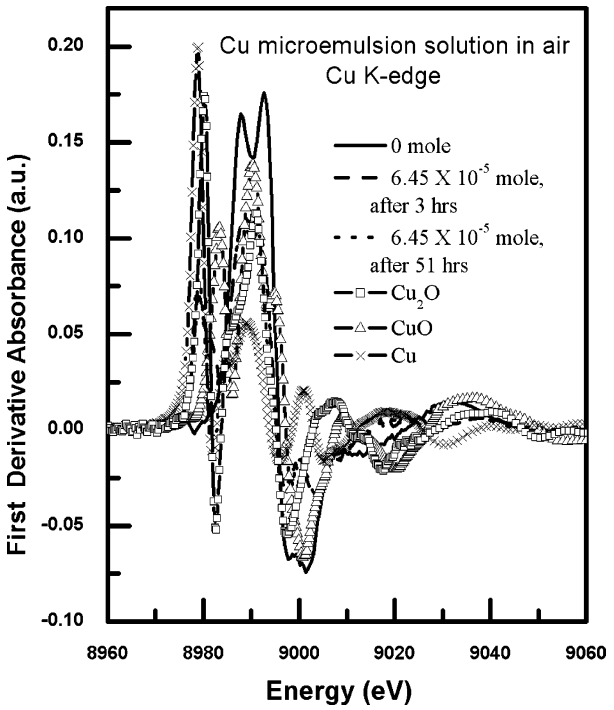

Figure 11. First derivative absorption spectra at the Cu K-edge of the Cu monometallic microemulsion system in air.

was allowed to stand for 51 h. At this point, we conclude that the Cu clusters are not effective catalysts for the reduction of dissolved oxygen in the solution. The XANES spectra at the Cu K-edge of Cu monometallic system in air can be taken as indirect evidence to support our findings of copper dissolution from the Pt surface of Pt−Cu clusters. Figure 11 shows that the adsorption jumps in Figure 10 have two different inflections corresponding to the derivative peaks at 8986 (α-peak) and 8991 (β-peak) eV. The main adsorption β-peak corresponds to the transition 1s → continuum. The α-peak located on the low energy side of the β-peak in Figure 11 is influenced by the degree of bond covalency and the degree of local structural disorder. On the basis of our understanding of the in situ XAS findings, we suggest that it may be possible to get the Pt-rich core and the Cu-rich shell bimetallic nanoparticles in AOT reverse microemulsions without Cu dissolution by a continuous supply of nitrogen gas during the preparation process.

The formation of Pt−Cu clusters was clearly observed step by step in this work. Comparing the FT EXAFS spectra of the Pt−Cu microemulsion system at the Pt L_{III}-edge, one can observe the Pt−Pt coordination after adding more than 1.93×10^{-3} mol of N_2H_4. The N_{Pt-Pt} value became larger if 2.81×10^{-3} mol of N_2H_4 was added to the Pt−Cu microemulsion system. Furthermore, the Pt−Pt coordination is still observable even if the solution is kept for a prolonged period such as 24 h. From the FT EXAFS spectra of the Pt−Cu microemulsion system at the Cu K-edge, one can observe the Cu−Pt coordination only after the addition of 2.81×10^{-3} mol of N_2H_4 with standing for 20 min. However, the Cu−Pt coordination disappeared if the system was kept for more than 3 h. From all of the observations, a model was proposed for the formation mechanism of Pt−Cu clusters at early stages, as shown in Scheme 1.

Five steps are proposed in this model. In the first step, the microemulsion system contains $PtCl_6^{2-}$ complex, Cu^{2+} ions, and the SO_3^- group of AOT. The $PtCl_6^{2-}$ complex ions are located in the center of the micelle before the addition of reducing agent.

SCHEME 1: Model Proposed for the Formation Mechanism of Pt−Cu Bimetallic Clusters at Early Stages

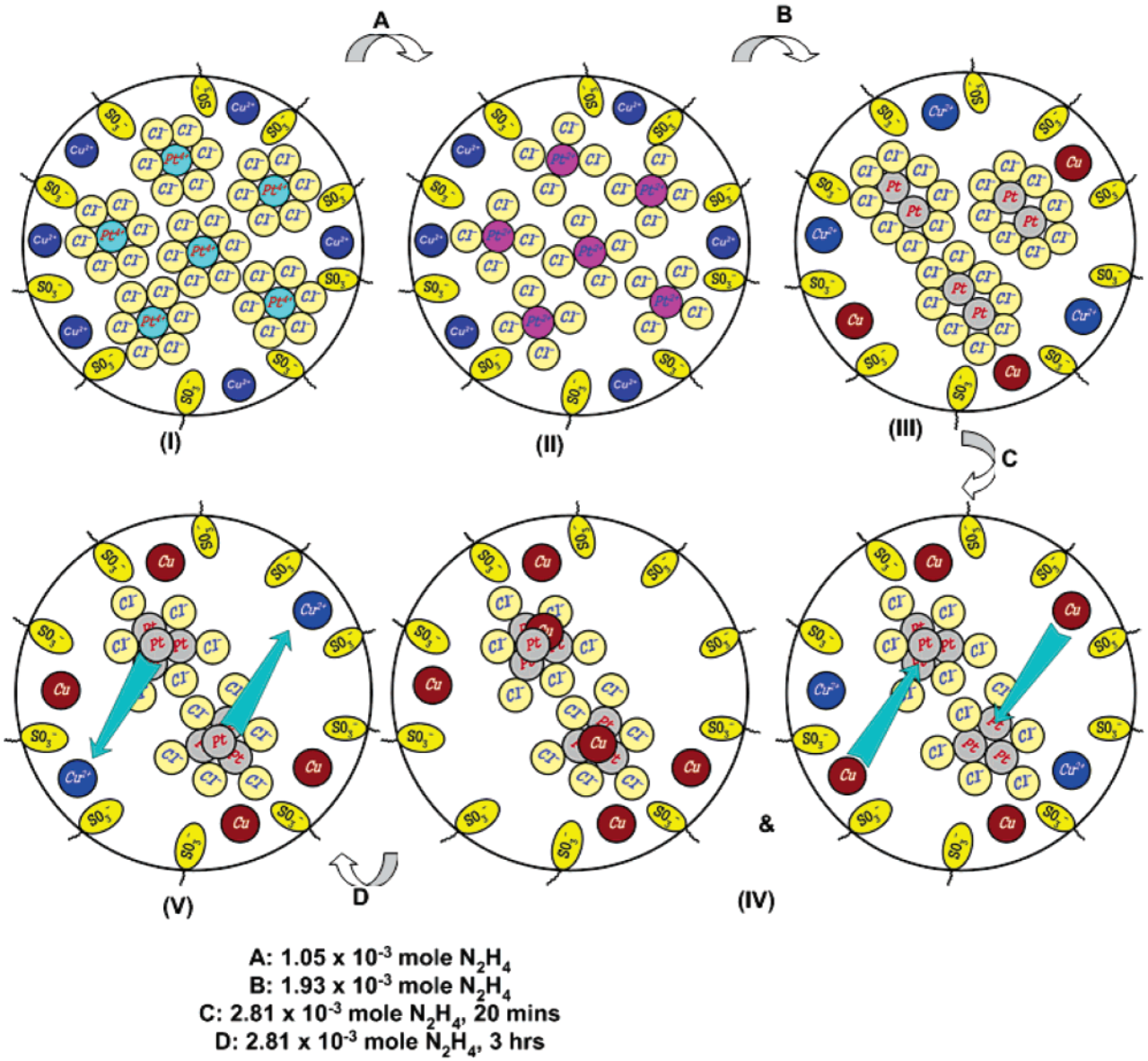

The Cu−O coordination number is around 4, indicating that the Cu^{2+} ions are located at the rear side of the micelle. There are two possibilities for copper ion coordination with oxygen. One explanation is that based on the well-known complex chemistry of copper, when copper nitrate was dissolved in a water pool of the reverse micelle, copper ions can exist either as a tetrahedral aqua complex $[Cu(H_2O)_4]^{2+}$ or as an octahedral complex $[Cu(H_2O)_6]^{2+}$. Another possibility is that copper ion may coordinate with the oxygen of the SO_3^- group of AOT. However, this possibility has less significance as per the infrared spectroscopy results of Camardo et al. on Cu^{2+} interactions with the SO_3^- group of AOT.[27] They found no variation in the frequency of the symmetric sulfonate stretching mode as the water-to-surfactant ratio is increased in the reverse micellar system. This indicates a less favorable interaction of Cu^{2+} with the SO_3^- anion. So, it is reasonable to assume that the Cu^{2+} ions were coordinated by the oxygen of the water molecules. After the addition of 1.05×10^{-3} mol of N_2H_4, in the second step, the $PtCl_6^{2-}$ ions were reduced through intermicellar exchange processes.[28,29] Reverse micelles in solution will exchange the contents in their cores via both fusion and redispersion processes.[30−33] As a result, reduction of metal salt within the cores of reverse micelles can result in the growth of nanosized metal particles. Subsequent particle growth depends strongly on exchange of the reactants between micelles. The exchange process occurs when micelles collide because of the Brownian motion or the attractive forces between the micelles. These collisions lead to a fusion of the reverse micelles, an exchange of the contents within the cores, and a redispersion of the micelles.[28,29,32,33] The value of N_{Pt-Cl} was found to reduce from 6 to around 4, revealing the formation of $PtCl_4^{2-}$ ions in this step. In the third step, after the addition of 1.93×10^{-3} mol of N_2H_4, the N_{Pt-Cl} and N_{Pt-Pt} became 3.8 and 1.2, respectively. However, no significant change is observed in N_{Cu-O} at this step. N_{Cu-Pt} is observed only in the fourth step, after the addition of 2.81×10^{-3} mol of N_2H_4 followed by standing for 20 min. In this step, the N_{Cu-O} value still remains unchanged. This observation indicates that a portion of Cu^{2+} ions is reduced to Cu^0 and adsorbed on Pt to form Pt−Cu clusters and the remaining Cu^{2+} ions are still located at the rear side of the micelle. At the final step, Pt atoms from the individual micelles aggregate together to form clusters of a larger size through intermicellar exchange processes when the microemulsion system is kept for a longer time of 3 h. However, the

Cu−Pt coordination is no more observed in this step, indicating the dissolution of Cu from the surface of Pt clusters.

Conclusion

This compilation of in situ XAS findings on Pt−Cu cluster formation in AOT reverse micelles reveals that the bimetallic clusters were formed through the successive reduction of metal ions as depicted in Scheme 1. In situ XAS results at the Pt L_{III}-edge revealed that the Pt^{4+} ions of the H_2PtCl_6 solution were reduced to Pt^{2+} first and then to Pt^0 to form Pt clusters in AOT reverse microemulsions. The Cu K-edge XAS results indicated the reduction of Cu^{2+} to Cu^0. It appears that the Cu clusters formed in the microemulsion were adsorbed on to the surface of the Pt as evidenced from the lower Cu−Pt coordination and absence of the Pt−Cu coordination. If the microemulsion system was allowed to stand for a longer period, Cu would be dissolved into solution from the Pt surface in the presence of dissolved oxygen. This evidence implied that Pt is an active catalyst for oxygen reduction leading to Cu oxidation and hence dissolution. In contrast, Cu would not be oxidized in the Cu monometallic microemulsion system even in the presence of air. These observations allowed us to conclude that the stability of Pt−Cu can be further improved if the synthesis would be carried out in the presence of air. Possible structural models were proposed to account for the XAS observations on the formation of Pt−Cu clusters in a microemulsion system at the early stages during the addition of various amounts of the reducing agent. On the whole, this work provides a detailed insight into the mechanism of nucleation and growth of Pt−Cu nanoclusters. Such information would be very helpful for a successful particle design and for a scaling-up process.

Acknowledgment. Financial support from the National Science Council (NSC-92-2811-E-011-008) and Ministry of Education (EX-92-E-FA09-5-4), National Taiwan University of Science and Technology, and National Synchrotron Radiation Research Center (NSRRC) is gratefully acknowledged.

References and Notes

(1) Sinfelt, J. H. *Bimetallic Catalysts-Discoveries, Concepts, and Applications*: *Exxon Monograph*; Wiley: New York, 1983.
(2) Sinfelt, J. H. *J. Catal*. **1973**, *29*, 308.
(3) Sinfelt, J. H. *Acc. Chem. Res*. **1989**, *20*, 134.
(4) Toshima. N. *J. Macromol. Sci. Chem*. **1990**, *A27*, 1225.
(5) Burch, R.; Garla, L. C. *J. Catal*. **1981**, *71*, 360.
(6) Biloen, P.; Helle, J. N.; Verbeek, H.; Dautzenberg, F. M.; Sachtler, W. M. H. *J. Catal*. **1980**, *63*, 112.
(7) Meitzner, G.; Via, G. H.; Lytle, F. W.; Sinfelt, J. H. *J. Chem. Phys*. **1985**, *83*, 4793.
(8) Harada, M.; Asakura, K.; Ueki, Y.; Toshima, N. *J. Phys. Chem*. **1992**, *96*, 9730.
(9) Toshima, N.; Harada, M.; Yamazaki, Y.; Asakura, K. J. *J. Phys. Chem*. **1992**, *96*, 9927.
(10) Davis, R. J.; Boudart, M. *J. Phys. Chem*. **1994**, *98*, 5471.
(11) McBreen, J.; Mukerjee, S. *J. Electrochem. Soc*. **1995**, *142*, 3399.
(12) Hills, C. W.; Nashner, M. S.; Frenkel, A. I.; Shapley, J. R.; Nuzzo, R. G. *Langmuir* **1999**, *15*, 690.
(13) Cimini, F.; Prins, R. *J. Phys. Chem. B* **1997**, *101*, 5285.
(14) Reifsnyder, S. N.; Lamb, H. H. *J. Phys. Chem. B* **1999**, *103*, 321.
(15) Tsai, Y. W.; Tseng, Y. L.; Sarma, L. S.; Liu, D. G.; Lee, J. F.; Hwang, B. J. *J. Phys. Chem. B* **2004**, *108*, 8148.
(16) Stern, E. A.; Newville, M.; Ravel, B.; Yacoby, Y.; Haskel, D. *Physica B* **1995**, *208*−*209*, 117.
(17) Zabinsky, S. I.; Rehr, J. J.; Ankudinov, A. L.; Albers, R. C.; Eller, M. J. *Phys. Rev. B* **1995**, *52*, 2995.
(18) Horsely, J. A. *J. Chem. Phys*. **1982**, *76*, 1451.
(19) Choi, E. Y.; Nam, I.; Kim, Y. G.; Chung, J. S.; Lee, J. S.; Nomura, M. *J. Mol. Catal*. **1991**, *69*, 247.
(20) Kau, L.-S.; Hodgason, K. O.; Solomon, E. I. *J. Am. Chem. Soc*. **1989**, *111*, 7103.
(21) *CRC Hand Book of Chemistry and Physics*, 80th ed.; Lide, D. R., Ed.; CRC Press: Boca Raton, FL, 1999−2000.
(22) Liu, C. M.; Guo, L.; Xu, H. B.; Wu, Z. Y.; Weber, J. *Microelectron. Eng.* **2003**, *66*, 107.
(23) Borthen, P.; Hwang, B. J.; Strehblow, H. H.; Kolb, D. M. *J. Phys. Chem. B* **2000**, *104*, 5078.
(24) Hwang, B. J.; Lin, S. H. *J. Electrochem. Soc*. **1995**, *142*, 3749.
(25) Markovic, N. M.; Gasteiger, H. A.; Grgur, B. N.; Ross, P. N. *J. Electroanal. Chem.* **1999**, *467*, 157.
(26) Toda, T.; Iganashi, H.; Watanabe, M. *J. Electrochem. Soc.* **1998**, *145*, 4185.
(27) Camardo, M.; D'Angelo, M.; Mannaioli, S.; Onori, G.; Santucci, A. *Colloids Surf., A* **1996**, *119*, 183.
(28) Hirai, T.; Sato, H.; Komasawa, I. *Ind. Eng. Chem. Res.* **1994**, *33*, 3262.
(29) Bagwe, R. P.; Khilar, K. C. *Langmuir* **1997**, *13*, 6432.
(30) Joshi, S. S.; Patil, S. F.; Iyer, V.; Mahumuni, S. *Nanostruct. Mater*. **1998**, *10*, 1135.
(31) Petit, C.; Jain, T. K.; Billoudet, F.; Pileni, M. P. *Langmuir* **1994**, *10*, 4446.
(32) Towey, T. F.; Khan-Lodhi, A.; Robinson, B. H. *J. Chem. Soc., Faraday Trans.* **1990**, *86*, 3757.
(33) Natarajan, U.; Handique, K.; Mehra, A.; Bellare, J. R.; Khilar, K. C. *Langmuir* **1996**, *12*, 2670.